FBS Effect and Temperature Dependence in Trench-Assisted Multimode Fiber

ZHANG Zelin[1,2], *LU Yuangang*[1,2*], *XIE Youwen*[1,2], *HUANG Jian*[1,2], *ZHOU Lang*[1,2]

1. Key Laboratory of Space Photoelectric Detection and Perception of Ministry of Industry and Information Technology, College of Astronautics, Nanjing University of Aeronautics and Astronautics, Nanjing 211106, P. R. China;
2. College of Science, Nanjing University of Aeronautics and Astronautics, Nanjing 211106, P. R. China

(Received 13 July 2020; revised 10 September 2020; accepted 12 September 2020)

Abstract: We propose the trench-assisted multimode fiber (TA-OM4) as a novel sensing fiber in forward Brillouin scattering (FBS)-based temperature sensor, due to its higher temperature sensitivity, better bending resistance and lower propagation loss, compared with the single mode fiber (SMF) and other sensing fibers. The FBS effect and acousto-optic interaction in TA-OM4 are the first time to be demonstrated and characterized at 1 550 nm theoretically and experimentally. A 2.0 km long TA-OM4 is put into an oven to measure its temperature sensitivity, which can reach up to 80.3 kHz/℃, exceeding 53% of SMF (52.4 kHz/℃). The simulated and experimental results verify that the TA-OM4 may be a good candidate as the sensing fiber for the FBS-based temperature sensor.

Key words: forward Brillouin scattering; acousto-optic interaction; optic-fiber sensor; temperature sensitivity; multimode fiber

CLC number: TN29 **Document code:** A **Article ID:** 1005-1120(2020)S-0095-07

0 Introduction

Stimulated Brillouin scattering (SBS) in optical fiber is a phenomenon caused by the interaction between a light wave and an acoustic wave, which is widely studied and employed in the field of distributed sensing[1-2]. Backward Brillouin scattering induces high frequency shifts around 10 GHz which can be utilized in Brillouin optical time-domain sensors and Brillouin laser. However, the forward Brillouin scattering (FBS) have much lower frequency shift of several hundreds of mega Hertz, which can be used in several applications, such as temperature sensing, opto-mechanical chemical sensors, optical frequency comb and opto-mechanical laser[3-6].

Recently, the temperature sensors based on FBS have been proposed using the silica single mode fiber (SMF), high nonlinear fiber (HNLF) and photonics crystal fiber (PCF)[7-9]. However, the lower temperature sensitivity of SMF may limit its measurement accuracy. Compared with SMF, although the HNLF and PCF have slightly lager temperature sensitivities, their disadvantages of bad bending resistance, high cost and large propagation loss which are 5.4 dB/km of PCF and 0.76 dB/km of HNLF, respectively, can compromise their sensing performance for future FBS-based temperature sensors in complex engineering application[8-9]. Fortunately, the trench-assisted multimode fiber (TA-OM4), due to its low propagation loss (0.24 dB/km) which is similar to that of SMF (0.20 dB/km), excellent bending resistance and high backward stimulated Brillouin scattering (BSBS) and modulation instability (MI) threshold, has been a good candidate as the sensing fiber in BSBS-based temperature sensors[10]. However, the characteristic of FBS process in TA-OM4 at 1 550 nm and its applications in FBS-based temperature sensors have

*Corresponding author, E-mail address: luyg@nuaa.edu.cn.

How to cite this article: ZHANG Zelin, LU Yuangang, XIE Youwen, et al. FBS effect and temperature dependence in trench-assisted multimode fiber[J]. Transactions of Nanjing University of Aeronautics and Astronautics, 2020, 37(S): 95-101.
http://dx.doi.org/10.16356/j.1005-1120.2020.S.012

not been reported.

In this paper, we theoretically and experimentally investigate the acousto-optic interaction caused by FBS and FBS spectrum in TA-OM4. Furthermore, we have found that the largest strain coefficient in TA-OM4 is about 4.0 kHz/με, which is so small that the frequency shift of FBS is not sensitive to make acceptable strain measurement. Therefore, we only focus on its temperature dependence of FBS in this paper. Compared with the temperature response of FBS in SMF, we experimentally measure the FBS temperature response of TA-OM4. The highest temperature dependence of TA-OM4 is linear with a coefficient of 80.3 kHz/℃, which is 53% larger than that of SMF (52.4 kHz/℃). The simulated and experimental results show that the TA-OM4 may be a good candidate as the sensing fiber in FBS-based temperature sensors.

1 FBS Resonances in TA-OM4

1.1 Theoretical description of FBS in optical fiber

The acoustic modes responsible for FBS are radial dilatational modes ($R_{0,m}$) and mixed torsional-radial modes ($TR_{2,m}$). The FBS is a typical opto-acoustic interaction, which can be described as the coupling amplitude equations between optical field $\boldsymbol{E}(\boldsymbol{r}, z, t)$ and acoustic wave for the displacement vector $\boldsymbol{U}(\boldsymbol{r}, z, t)$ [11]

$$\frac{\partial^2 \boldsymbol{E}}{\partial z^2} - \frac{n_{\text{eff}}^2}{c^2}\frac{\partial^2 \boldsymbol{E}}{\partial t^2} = \frac{1}{\varepsilon_0 c^2}\frac{\partial^2 \boldsymbol{P}^{\text{NL}}}{\partial t^2} \tag{1}$$

$$\frac{\partial^2 \boldsymbol{U}}{\partial z^2} + \Gamma\frac{\partial \boldsymbol{U}}{\partial t} + V_s{}^2\nabla\times(\nabla\times\boldsymbol{U}) - V_l{}^2\nabla(\nabla\cdot\boldsymbol{U}) = \frac{\boldsymbol{F}}{\rho_0} \tag{2}$$

where $\boldsymbol{P}^{\text{NL}}$ is the total nonlinear polarization, c the light velocity in vacuum, n_{eff} the effective refractive index, ε_0 the vacuum permittivity, V_l the longitudinal acoustic velocity of the fiber, ρ_0 the density of fused silica, V_s shear sound velocity of the fiber, and Γ the acoustic damping parameter. $\boldsymbol{F} = \varepsilon_0[1/2\gamma_{12}\nabla(\boldsymbol{E}\cdot\boldsymbol{E}) + \gamma_{44}(\boldsymbol{E}\cdot\nabla)\boldsymbol{E}]$ is the electrostrictive driving term, and γ_{12} and γ_{44} are both the elements of the electrostrictive tensor for fused silica. By employing the finite element analysis (FEA) method and solving Eq.(1), we obtain the optical field $E(r)$. Moreover, by solving Eq.(2) with the appropriate boundary conditions, we difine the normalized displacement distribution $U_m(r)$ in terms of Bessel functions $J_n(z)$, where n is the order of Bessel functions. By using $\rho_m(r) = -\rho_0\nabla U_m(r)$, we obtain the density vibration caused by FBS.

For the radial dilatational $R_{0,m}$ modes, the boundary condition corresponding to the free fiber surface can be written as

$$(1-\alpha^2)J_0(y) - \alpha^2 J_2(y) = 0 \tag{3}$$

where α is the ratio between shear sound velocity and longitudinal acoustic velocity, and y_m the mth zero of Eq.(3). Furthermore, the central frequency of the mth acoustic mode can be expressed as

$$f_m = \frac{y_m V_l}{\pi d} \tag{4}$$

where d is the cladding diameter of optical fiber.

Similar to the Kerr effect in fiber, the opto-mechanical coefficient can be used to quantify the opto-acoustic interaction caused by FBS, which can be expressed as[6,12-13]

$$\gamma_{\text{OM}}^{(m)} = \frac{k_0}{2\pi n_{\text{neff}}^2 c\rho_0}\frac{Q_E^{(m)}Q_p^{(m)}}{\Gamma_m f_m} \tag{5}$$

where Γ_m is the linewidth of the mth resonant peak induced by FBS. The $Q_E^{(m)}$ and $Q_p^{(m)}$ are the electrostrictive overlap and photo-elastic overlap, which determines the efficiency of stimulation of acoustic modes and describes the modification of the effective index by acoustic modes[13-14], respectively. By solving Eqs.(1)—(5), the acoustic field distribution and FBS resonances can be obtained next.

1.2 Simulation and FBS spectrum in TA-OM4

For TA-OM4, the diameters of the fiber core and cladding are 50 and 125 μm, respectively. The refractive index profile is given in Fig.1. The refractive index profile shows a quasi-quadratic distribution in the central region and has a trench-index profile around the fiber core[10]. The three highest linear polarization (LP) modes are respectively LP_{01},

LP_{11} and LP_{21}, and the corresponding intensity ratio of these three LP modes $I_{01}:I_{11}:I_{21}$, is 1:0.14:0.006. Considering the highest intensity ratio of LP_{01}, the tiny coupling efficiency between LP_{01} and other high-order modes and the single mode condition of most optical components[15], it is enough to investigate the FBS process of TA-OM4 corresponding to the fundamental mode LP_{01}.

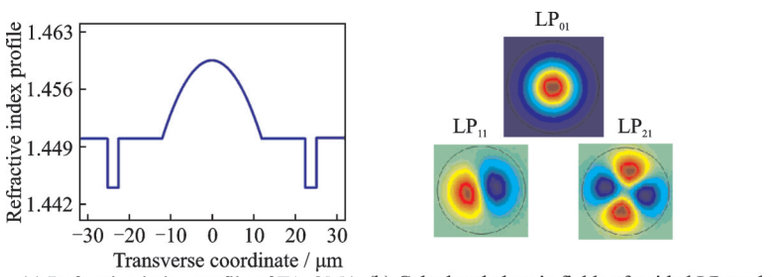

(a) Refractive index profile of TA-OM4 (b) Calculated electric fields of guided LP mode LP_{01}, LP_{11} and LP_{21} at 1 550 nm in TA-OM4

Fig.1 Refractive index profile of TA-OM4 and calculated three LP optical modes with the highest intensity

By solving Eqs. (1) and (2), three excited acoustic modes are found and displayed in Fig. 2. As it shown in Fig.2(a), taking $R_{0,4}$ mode as an example, the $R_{0,m}$ modes are the radial dilatational modes, which have the most efficient scattering efficiency and are independent of angular coordinate φ. Especially, the $R_{0,m}$ modes can induce refractive index changes so that the pure phase modulation will be also induced. Other acoustic modes are $TR_{2,m}$ acoustic modes, which are the mixed torsional-radial modes. As it shown in Figs.2(b) and (c), different from $R_{0,m}$ modes, the $TR_{2,m}$ modes are doubly degenerated, which vary sinusoidally with angular coordinate 2φ. Furthermore, the scattering efficiency of $TR_{2,m}$ modes is much lower than that of $R_{0,m}$ modes. For the $TR_{2,m}$ (90°/0°) mode, its induced birefringent axes are parallel to the birefringent axes of TA-OM4, which does not induce the depolarized scattering but the polarized scattering and also cause pure phase modulation. For the $TR_{2,m}$ (45°/−45°) mode, the mode pattern is rotated by 45°. In this case pure phase modulation will not occur, and the depolarized scattering is induced[16].

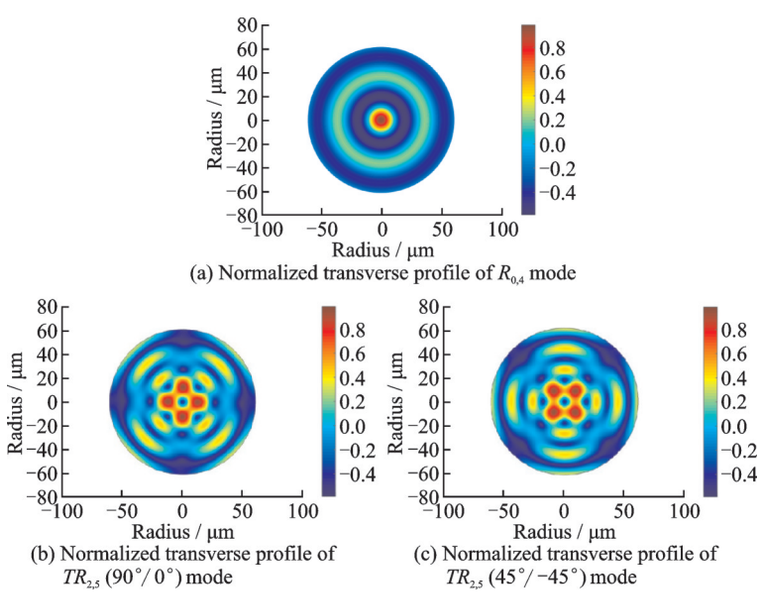

(a) Normalized transverse profile of $R_{0,4}$ mode

(b) Normalized transverse profile of $TR_{2,5}$ (90°/0°) mode

(c) Normalized transverse profile of $TR_{2,5}$ (45°/−45°) mode

Fig.2 Normalized transverse profile of acoustic modes excited by LP_{01} optical mode in TA-OM4

Generally, the overlap between optical modes and acoustic modes determines the shape of FBS resonances. Taking four acoustic modes ($R_{0,1}$ to $R_{0,4}$) as examples, the 2D mode profiles of longitudinal optical fundamental mode LP_{01} and four acoustic modes are displayed in Fig.3.

In order to experimentally investigate the FBS process in TA-OM4, we also measure the FBS spectrum by using a coherent detection, which is shown in Fig.4. The light source (NKT Photonics) is a 1 550 nm single-wavelength semiconductor laser with linewidth 5 kHz. The pump light propagating through the isolator (ISO) is split into two branches by a 50/50 coupler. The upper branch used as the pump light is amplified by an erbium-doped fiber amplifier (EDFA, Amonics). A narrow bandpass filter (BPF, AOS Photonics) with 3.5 GHz bandwidth is used to eliminate the amplified spontaneous emission (ASE) noise induced by EDFA. A variable attenuator (VA) is utilized to adjust the input power level to protect fiber components. The pump light is launched into 2.0 km long TA-OM4 (YOFC) to obtain the FBS signal which beats with the reference light. Finally, a 1.6 GHz bandwidth photodetector (PD, Thorlabs PDB480) is utilized to detect the beat signal, which is analyzed by an electrical spectrum analyzer (ESA, Tektronix RSA5126B) and used to obtain the FBS spectrum.

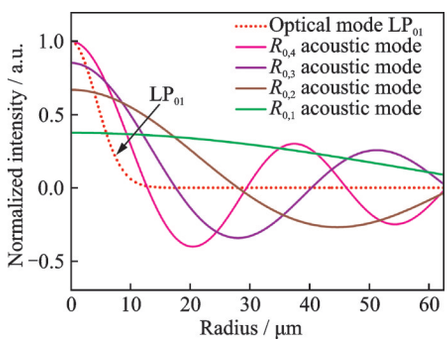

Fig.3 2-D profiles of optical mode LP_{01} and acoustic modes $R_{0,1}$ to $R_{0,4}$

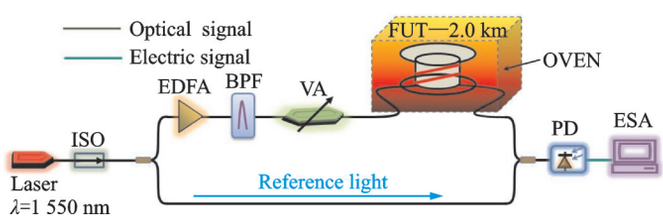

Fig.4 Experimental setup of measuring the FBS spectrum of TA-OM4

In our experiment, the incident light power is 11.2 mW. The measured FBS spectrum is shown in Fig.5. The measured FBS spectrum includes two parts. One part is from the $R_{0,m}$ modes and the other is from the $TR_{2,m}$ modes. However, due to the random change of polarization states along the TA-OM4, the FBS intensities induced by $TR_{2,m}$ modes are much lower than those of $R_{0,m}$ modes. As it shown in Fig.5, we can find that the fourth resonant peak with the highest intensity locates at 173.1 MHz. By solving Eq.(5), we obtain the calculated opto-mechanical coefficient of $R_{0,4}$ mode as 5.25 $(W\cdot km)^{-1}$, which is slightly higher than that of SMF 5 $(W\cdot km)^{-1}$[6]. In Fig.6, two adjacent resonant peaks generated by $R_{0,m}$ modes have equivalent frequency interval of 47.5 MHz, which can be verified by solving Eq.(4). It is obvious that, whatever resonant peaks intensity and frequency shift, the calculated and experimental results are in good agreement. The largest difference of normalized intensity between calculated and experimental results are less than 5%, which are from the error of the estimated fiber parameters.

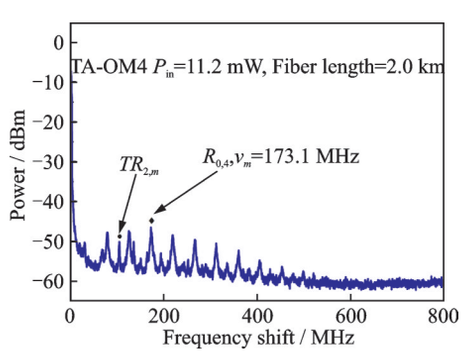

Fig.5 The measured FBS spectrum of TA-OM4

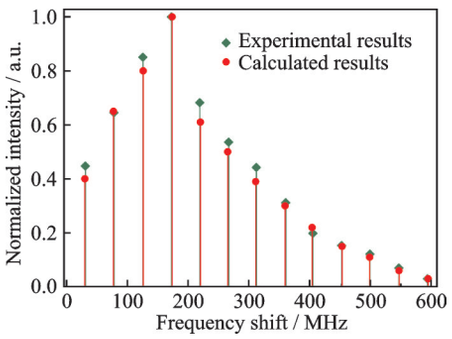

Fig.6 Measured (green) and calculated (red) normalized FBS resonant intensity in TA-OM4 induced by $R_{0,m}$ modes

2 Temperature Response in TA-OM4

In order to evaluate whether the TA-OM4 can be used as the novel sensing fiber in FBS-based temperature sensors, we put both TA-OM4 and SMF into an oven to measure their temperature sensitivities of $R_{0,m}$ modes, and results are shown in Fig.7. Seven different temperatures between −10 ℃ to 50 ℃ are measured with a temperatures step of 10 ℃. It is obvious that the temperature sensitivities increase linearly with an increase in m value of $R_{0,m}$ modes, whose trends are in accordance with that in Ref.[17]. The observed temperature coefficient of $R_{0,12}$ in TA-OM4 can reach 80.3 kHz/℃, which is 53% larger than that of SMF (52.4 kHz/℃).

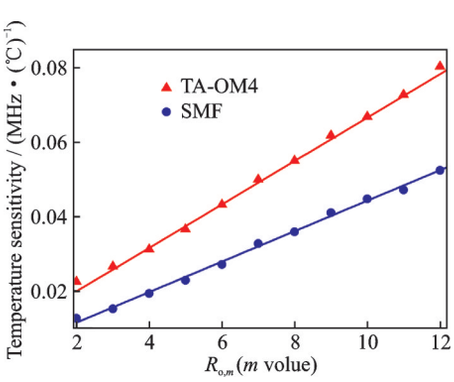

Fig.7 Measured temperature sensitivities of TA-OM4 and SMF versus different $R_{0,m}$ modes, respectively

Furthermore, we also obtain the temperature sensitivities of spectral peaks corresponding to $R_{0,4}$ (f_4=173.1 MHz) mode in TA-OM4 and $R_{0,5}$ (f_5=222.9 MHz) mode in SMF, which exhibit the highest resonance intensity of all peaks. In Fig.8, the calibration temperature coefficient of TA-OM4 ($\alpha_{\text{TA-OM4}}$) can reach 31.9 kHz/℃, which is much 41% larger than that of SMF (α_{SMF} =22.6 kHz/℃).

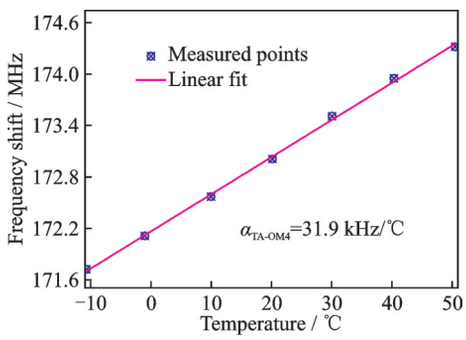

(a) Frequency shift induced by $R_{0,4}$ mode as a function of temperature in TA-OM4

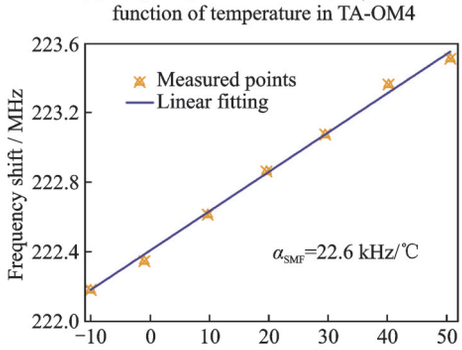

(b) Frequency shift induced by $R_{0,5}$ mode as a function of temperature in SMF

Fig.8 Temperature sensitivities of $R_{0,4}$ mode in TA-OM4 and $R_{0,5}$ mode in SMF

3 Conclusions

FBS processes in TA-OM4 are theoretically and experimentally investigated and the acousto-optic interaction of TA-OM4 at 1 550 nm are characterized and demonstrated. We experimentally measure the FBS spectrum, which is in good agreement with simulated results. The temperature sensitivities of $R_{0,m}$ modes in TA-OM4 are also measured, which exceed 40% of SMF. The calculated and experimental results demonstrate that the TA-OM4 could be a good sensing fiber in FBS-based temperature sensors, with advantages of high temperature sensitivity, good bending resistance and low propagation loss.

References

[1] MATSUI T, NAKAJIMA K, YAMAMOTO F. Guided acoustic-wave brillouin scattering characteris-

tics of few-mode fiber[J]. Applied Optics, 2015, 54(19): 6093-6097.

[2] BAO X, CHEN L. Recent progress in Brillouin scattering based fiber sensors[J]. Sensors, 2011, 11(4): 4152-4187.

[3] FU Y, FAN X, WANG B, et al. Discriminative measurement of temperature and strain using stimulated Brillouin scattering and guided acoustic-wave brillouin scattering[C]//2018 Asia Communications and Photonics Conference (ACPC). Hangzhou: IEEE, 2018: 1-3.

[4] CHOW D M, THEVENAZ L. Opto-acoustic chemical sensor based on forward stimulated Brillouin scattering in optical fiber (Invited)[C]//Proceedings of the 7th International Conference on Photonics (ICP). [S.l.]:IEEE, 2018: 1-3.

[5] BUTSCH A, KOEHLER J R, NOSKOV R E, et al. CW-pumped single-pass frequency comb generation by resonant optomechanical nonlinearity in dual-nanoweb fiber[J]. Optica, 2014, 1(3): 158-164.

[6] LONDON Y, DIAMANDI H H, ZADOK A. Electro-opto-mechanical radio-frequency oscillator driven by guided acoustic waves in standard single-mode fiber[J]. APL Photonics, 2017, 2(4): 041303.

[7] YAIR A, LONDON Y, ZADOK A. Scanning-free characterization of temperature dependence of forward stimulated Brillouin scattering resonances[C]//Proceedings of the 24th International Conference on Optical Fiber Sensors (ICOFS). Curitlba: SPIE, 2015: 96345C.1-96345C.4.

[8] HAYASHI N, SUZUJI K, SET S Y, et al. Temperature coefficient of sideband frequency produced by polarized guided acoustic-wave Brillouin scattering in highly nonlinear fibers[J]. Applied Physics Express, 2017, 10(9): 092501.1-092501.3.

[9] CARRY E, BEUGNOT J C, STILLER B, et al. Temperature coefficient of the high-frequency guided acoustic mode in a photonic crystal fiber[J]. Applied Optics, 2011, 50(35):6543-6547.

[10] ZHANG Z L, LU Y G. Trench-assisted multimode fiber used in Brillouin optical time domain sensors[J]. Optics Express, 2019, 27(8): 11396-11405.

[11] KANG M S, BRENN R, RUSSELL R S J. All-optical control of gigahertz acoustic resonances by forward stimulated inter-polarization scattering in a photonic crystal fiber[J]. Physical Review Letters, 2010, 105(15): 153901.1-153901.4.

[12] BUTSCH A, KANG M S, EUSER T G, et al. Optomechanical nonlinearity in dual-nanoweb structure suspended inside capillary fiber[J]. Physical Review Letters, 2012, 109(18): 183904.1-183904.5.

[13] DIAMANDI H H, LONDON Y, ZADOK A. Opto-mechanical inter-core cross-talk in multi-core fibers[J]. Optica, 2017, 4(3): 289.

[14] BIRYUKOV A S, SUKHAREV M E, DIANOV E M. Excitation of sound waves upon propagation of laser pulses in optical fibers[J]. Quantum Electronics, 2002, 32(9): 765-775.

[15] XU Y, REN M, LU Y, et al. Multi-parameter sensor based on stimulated Brillouin scattering in inverse-parabolic graded-index fiber[J]. Optics Letters, 2016, 41(6): 1138-1141.

[16] NISHIZAWA N, KUME S, MORI M, et al. Experimental analysis of guided acoustic wave Brillouin scattering in PANDA fibers[J]. Journal of the Optical Society of America B, 1995, 12(9): 1651-1655.

[17] CHUN Y D, SHANG L H, JING L L, et al. Simultaneous measurement on strain and temperature via guided acoustic-wave Brillouin scattering in single mode fibers[J]. Acta Physica Sinica, 2016, 65(24). 240702. 1-240702.7.

Acknowledgements This work was supported in part by the National Natural Foundation of China (Nos. 61875086, 61377086), the Aerospace Science Foundation of China (No.2016ZD52042), and Nanjing University of Aeronautics and Astronautics Ph. D. short-term visiting scholar project (No.190901DF08).

Authors Mr. **ZHANG Zelin** is currently a Ph. D. candidate of Optical Engineering at the Department of Applied Physics, Nanjing University of Aeronantics and Astronautics (NUAA). His research focuses on distributed fiber sensors and nonlinear fiber optics.

Prof. **LU Yuangang** is currently a professor in College of Astronautics at NUAA. His research focuses on distributed fiber sensors, image processing and technology of photoelectrical detection.

Author contributions Mr. **ZHANG Zelin** contributed to simulation by doing experiment and writing the manuscript. Prof. **LU Yuangang** designed and guided the study, and gave key opinions on the core issues. Mr. **XIE Youwen** and Mr. **HUANG Jian** conducted some related works about the experiments. Ms. **ZHOU Lang** conducted some related works about the simulation.

Competing interests The author declare no competing interests.

(Production Editor: XIA Daojia)

沟道型折射率多模光纤的前向布里渊散射效应及其温度响应

张泽霖[1,2]，路元刚[1,2]，谢有文[1,2]，黄　剑[1,2]，周　朗[1,2]

（1.空间光电探测与感知工业和信息化部重点实验室，南京航空航天大学航天学院，南京 211106，中国；
2.南京航空航天大学理学院，南京 211106，中国）

摘要：提出了沟道型折射率多模光纤（TA-OM4）可作为一种新型传感光纤应用于基于前向布里渊散射（FBS）的温度传感器中。同单模光纤（SMF）和其他传感光纤相比，TA-OM4多模光纤具有高温度响应、抗弯曲和低传输损耗的优良特性。从理论和实验上对TA-OM4多模光纤在1 550 nm光波长下的FBS效应进行了研究。同时温度响应测试发现，TA-OM4的温度-频移系数可高达80.3 kHz/℃，比单模光纤的温度-频移系数（52.4 kHz/℃）高53%以上。

关键词：前向布里渊散射；声光互作用；光纤传感器；温度敏感性；多模光纤